Sciencexpress Report

Imaging Doped Holes in a Cuprate Superconductor with High-Resolution Compton Scattering

Y. Sakurai,[1]* M. Itou,[1] B. Barbiellini,[2] P. E. Mijnarends,[2,3] R. S. Markiewicz,[2] S. Kaprzyk,[2,4] J. -M. Gillet,[5] S. Wakimoto,[6] M. Fujita,[7] S. Basak,[2] Yung Jui Wang,[2] W. Al-Sawai,[2] H. Lin,[2] A. Bansil,[2] K. Yamada,[7,8]

[1]Japan Synchrotron Radiation Research Institute (JASRI), SPring-8,1-1-1 Kouto, Sayo, Hyogo 679-5198, Japan. [2]Physics Department, Northeastern University, Boston, Massachusetts 02115, USA. [3]Department of Radiation, Radionuclides & Reactors, Faculty of Applied Sciences, Delft University of Technology, Delft, The Netherlands. [4]Academy of Mining and Metallurgy AGH, 30059 Kraków, Poland. [5]Ecole Centrale Paris, SPMS UMR CNRS 8580, Grande Voie des Vignes, 92295 Châtenay-Malabry, France. [6]Quantum Beam Science Directorate, Japan Atomic Energy Agency, Tokai, Naka, Ibaraki 319-1195, Japan. [7]Institute for Materials Research, Tohoku University, Sendai 980-8577, Japan. [8]Advanced Institute for Materials Research, Tohoku University, Sendai 980-8577, Japan.

*To whom correspondence should be addressed; E-mail: sakurai@spring8.or.jp

The high temperature superconducting cuprate, $La_{2-x}Sr_xCuO_4$ (LSCO), shows several phases ranging from antiferromagnetic insulator to metal with increasing hole doping. To understand how the nature of the hole state evolves with doping, we have carried out high-resolution Compton scattering measurements at room temperature together with first-principles electronic structure computations on a series of LSCO single crystals in which the hole doping level varies from the underdoped (UD) to the overdoped (OD) regime. Holes in the UD system are found to primarily populate the O $2p_x/p_y$ orbitals. In contrast, the character of holes in the OD system is very different in that these holes mostly enter Cu-*d* orbitals. High-resolution Compton scattering provides a bulk-sensitive method for imaging the orbital character of dopants in complex materials.

The evolution of the electronic structure as well as the orbital character of the doped carriers is a key ingredient for understanding the physics of the cuprates and the mechanism of high-temperature superconductivity. Photoemission has succeeded in obtaining detailed information on the electronic dispersion and Fermi surface topology (*1*–*3*). Concerning the orbital character, comprehensive studies have concluded that the doped holes predominantly enter into the oxygen 2*p* orbital in the cuprates, at least up to optimal doping (*4*–*7*). As a result, the unusual physical properties of underdoped (UD) cuprates have been analyzed mainly by ascribing a single orbital character to the doped holes. However, in the overdoped (OD) cuprates the orbital character is not fully understood, even though distinct doping dependencies of x-ray absorption (*8*, *6*) and optical reflectivity spectra (*9*) suggest a change in the oxygen 2*p* orbital character with overdoping. In order to detect changes in orbital character with doping, we need to consider spectral differences, which requires high quality data for extracting weak wave function effects. Moreover, it is essential to measure a physical quantity which is connected to wave functions, such as the electron momentum density (EMD). Compton scattering is one of the most promising techniques for probing the orbital character of doped holes because it allows direct access to the EMD (*10*). Advantages of Compton scattering over other spectroscopies are that we do not need a nearly defect-free single crystal or a clean surface or ultra high vacuum, and the matrix element involved is much simpler than in other highly resolved spectroscopies such as photoemission (*11*), resonant inelastic X-ray scattering (*12*), scanning tunneling (*13*) and positron-annihilation (*14*). X-ray Compton scattering has established itself as a viable technique for investigating orbital character (*15*, *16*) and Fermi surface geometry of the bulk system (*17*–*20*) in wide classes of materials.

We have obtained two-dimensional electron momentum densities (2D-EMDs), which represent one-dimensional integrals along the c-axis of three-dimensional EMDs for single crystalline samples of $La_{2-x}Sr_xCuO_4$ with four different hole dopings, x=0.0, 0.08, 0.15 and 0.30 at room temperature. The samples and measurements are described in (*21*) and the experimental 2D-EMDs are presented in fig. S1. To clarify the evolving character of doped holes, the differences in 2D-EMD between two samples with different doping levels have been taken. This subtraction technique (Fig. 1) provides information on changes in orbital occupation numbers associated with doped holes (*22*). Subtraction acts as a projector on an energy slice near the Fermi level with the advantage of eliminating the large isotropic contribution of the core as well as irrelevant valence electrons. Each electronic state has its own angular dependence in momentum space which facilitates the detection of the state. For an atomic orbital, the EMD, which is the squared modulus of the

momentum-space wave function, has the same point symmetry as the corresponding charge density. This result carries over to molecular states (*23*)and is equally applicable to solid state wave functions (*24*). The radial behavior of the momentum-space wave function for each atomic orbital is determined by the spherical Bessel function, which behaves as p^l at small momenta p, where l is the orbital quantum number (*25*). Therefore, oxygen 2*p* bands contribute to the EMD at low momenta, while the contribution of the Cu 3*d* bands increases as p^4. This means that O 2*p* states are more visible in the 1st Brillouin Zone (BZ) while Cu 3*d* states are better seen in higher BZs.

An important question regarding the nature of the electronic ground state of LSCO is the character of the extra holes introduced when we dope the half-filled insulator. Zhang and Rice (*7*) suggested that the holes reside in a molecular orbital state, $P_{ZR}=P_{1x}-P_{2y}-P_{3x}+P_{4y}$ (Fig. 2A), where numbers 1 to 4 label the four O atoms and subscript *x*/*y* denotes the direction of the O 2*p* orbital involved in the plaquette of four O atoms surrounding a Cu atom in the CuO_2 plane. The molecular orbital P_{ZR} couples with the Cu $3d_{x^2-y^2}$ state and forms the so-called Zhang-Rice singlet. By enhancing the O character of the doped hole near half filling, the Zhang-Rice singlet has a strong impact on Compton scattering. In cuprates the angular dependence of the wave functions is primarily set by the *d*-orbitals of Cu, which hybridize with properly symmetrized combinations of *p* orbitals on nearest-neighbor oxygens. Hence we separate the strong peaks in Fig. 1 into peaks along the [100] axes associated with predominantly Cu $3d_{x^2-y^2}$ states, and other peaks along the diagonal directions assigned to the Cu $3d_{z^2}$ orbital hybridized with the molecular orbital $P_0=P_{1x}+P_{2y}+P_{3x}+P_{4y}$ (Fig. 2D). The Cu $3d_{z^2}$ state can also mix with the p_z atomic orbital from the apical oxygen. A two-orbital model which incorporates both e_g bands, namely the z^2 and the x^2-y^2 hybrid bands, captures several crucial properties of LSCO (*26*).

Figure 2 shows that a number of features of the momentum density of Fig. 1 can be understood in a simple molecular orbital picture (*22*) in which band structure details are neglected. By varying the relative Cu character of the orbital, the model properly describes the doping evolution of the Zhang-Rice characteristics (Figs. 2B-C), as well as features of the z^2 states (Figs. 2E-2F). However, because of the finite molecular size, the calculations do not quantitatively reproduce the radial positions of O and Cu features in momentum space. These features are more correctly described by band structure calculations, despite the fact that these calculations do not properly reproduce the doping evolution of Cu-O hybridization. Details of the EMD patterns are determined by competition between two opposing tendencies. Coulomb repulsion tends to localize *d* electrons on the Cu atoms while mixing with the oxygen *p* electron states tends to delocalize these same electrons. Band-structure and molecular orbital calculations are thus both useful for identifying various features in the Compton spectra. The band diagram in Fig. 3A shows the two main bands near the Fermi level. The band with x^2-y^2 symmetry is higher in energy than the band of z^2 symmetry. By calculating difference spectra over appropriate energy intervals, we can determine the patterns associated with particular orbitals. As shown in Fig. 3B, experiment and theory show a reasonable agreement regarding the difference of the directional Compton profiles [100]-[110] for x=0.15. The present theoretical Compton profiles are computed from the Green functions obtained by Korringa-Kohn-Rostoker Coherent Potential Approximation (KKR-CPA) calculations within the Local Density Approximation (LDA) (*27*, *28*, *21*), which yields Fermi surface properties in agreement with ARPES experiments (*1*). Figure 3 also shows the contribution of the 2D-EMDs between -0.4 eV and +0.1 eV from the x^2-y^2 band (Fig. 3C), between -0.8 eV and -0.4 eV from the z^2 band (Fig. 3D), and between -0.8 eV and +1.3 eV from both bands (Fig. 3E). These calculations reproduce trends related to the Cu-O states. Notably, in Fig. 3E the two diagonal features approximately agree with the experimental Fig. 1C despite some discrepancies regarding the position of the Cu *d* features along p_x and p_y. Interestingly, other small experimental features along these directions, which are related to d_{xz} and d_{yz} orbitals, could be found at lower energy in the theory. In any event, the present analysis in the energy range between -0.8 eV and +1.3 eV clearly captures the dominant features of the two-orbital band model (*26*). Part of the disagreement between theory and experiment is related to the fact that our LDA computations tend to underestimate the d_z^2 character of states at the Fermi energy (*29*). Our analysis shows that for small Sr concentrations the doped holes have a substantially greater O 2*p* character than predicted by band-theory. These effects are difficult to describe within the conventional Fermi liquid picture and would likely require the treatment of electron correlations involving the formation of Zhang-Rice singlets (*7*). We note as well that lattice perturbations affecting the bonding properties such as Jahn-Teller distortions and polaronic displacements are not included in the present calculations.

Our study shows the use of high-resolution Compton scattering for direct, bulk-sensitive imaging of the orbital character of dopants in the ground state of complex materials. This information cannot be obtained from other highly resolved spectroscopies. Features in Compton spectra are extremely robust since they are not significantly affected by defects, surfaces or impurities.

References and Notes

1. S. Sahrakorpi, M. Lindroos, R. S. Markiewicz, A. Bansil, *Phys. Rev. Lett.* **95**, 157601 (2005).
2. A. Damascelli, Z. Hussain, Z.-X. Shen, *Rev. Mod. Phys.* **75**, 473 (2003).
3. T. Yoshida *et al.*, *Phys. Rev. B* **74**, 224510 (2006).
4. N. Nücker *et al.*, *Phys. Rev. B* **39**, 6619 (1989).
5. A. Bianconi *et al.*, *Solid State Commun.* **63**, 1009 (1987).
6. C. T. Chen *et al.*, *Phys. Rev. Lett.* **68**, 2543 (1992).
7. F. C. Zhang, T. M. Rice, *Phys. Rev. B* **37**, 3759 (1988).
8. D. C. Peets *et al.*, *Phys. Rev. Lett.* **103**, 087402 (2009).
9. S. Uchida *et al.*, *Phys. Rev. B* **43**, 7942 (1991).
10. M. J. Cooper, P. E. Mijnarends, N. Shiotani, N. Sakai, A, Bansil (eds), *X-ray Compton Scattering*, (Oxford University Press), (2004).
11. A. Bansil, M. Lindroos, *Phys. Rev. Lett.* **83**, 5154 (1999).
12. R.S. Markiewicz and A. Bansil, Phys. Rev. Lett. **96**, 107005 (2006).
13. J. Nieminen, H. Lin, R. S. Markiewicz, and A. Bansil, Phys. Rev. Lett. **102**, 037001 (2009).
14. L. C. Smedskjaer, A. Bansil, U.Welp, Y. Fang, and K.G. Bailey, J. Phys. Chem. Solids **52**, 1541 (1991).
15. A. Koizumi *et al.*, *Phys. Rev. Lett.* **86**, 5589 (2001).
16. B. Barbiellini *et al.*, *Phys. Rev. Lett.* **102**, 206402 (2009).
17. Y. Sakurai *et al.*, *Phys. Rev. Lett.* **74**, 2252 (1995).
18. S. B. Dugdale *et al.*, *Phys. Rev. Lett.* **96**, 046406 (2006).
19. N. Hiraoka, T. Buslaps, V. Honkimäki, J. Ahmad, H. Uwe, *Phys. Rev. B* **75**, 121101(R) (2007).
20. C. Utfeld *et al.*, *Phys. Rev. B* **81**, 064509 (2010).
21. Materials and methods are available as supporting material on *Science* Online.
22. B. Barbiellini *et al.*, *Physica C: Superconductivity* **229**, 113 (1994).
23. W. Weyrich, P. Pattison, B. G. Williams, *Chem. Phys.* **41**, 271 (1979).
24. R. Harthoorn, P. E. Mijnarends, *J. Phys. F: Metal Phys.* **8**, 1147 (1978).
25. P. E. Mijnarends, *Physica* **63**, 235 (1973).
26. H. Sakakibara, H. Usui, K. Kuroki, R. Arita, H. Aoki, *Phys. Rev. Lett.* **105**, 057003 (2010).
27. A. Bansil, R. S. Rao, P. E. Mijnarends, L. Schwartz, *Phys. Rev B* **23**, 3608 (1981).
28. A. Bansil, *Zeitschrift Naturforschung A* **48**, 165 (1993).
29. J. B. Goodenough, J. Zhou, *Phys. Rev. B* **42**, 4276 (1990).

Acknowledgments: The work at JASRI was supported by a Grant-in-Aid for Scientific Research (No. 18340111) from the Ministry of Education, Culture, Sports, Science, and Technology (MEXT), Japan, and that at Tohoku University was supported by a Grant-in-Aid for Scientific Research (Nos. 16104005, 19340090, 22244039) from the MEXT, Japan. The work at Northeastern University (NU) was supported by the Division of Materials Science and Engineering, Office of Science, U.S. Department of Energy, and it benefited from the allocation of supercomputer time at NERSC, the NU's Advanced Scientific Computation Center (ASCC), and the Stichting Nationale Computerfaciliteiten (National Computing Facilities Foundation, NCF). The Compton scattering experiments were performed with the approval of JASRI (Proposals, 2003B0762, 2004A0152, 2007B1413, 2008A1191, 2010A1907).

Supporting Online Material

www.sciencemag.org/cgi/content/full/science.1199391/DC1
Materials and Methods
Fig. S1

21 October 2010; accepted 22 March 2011
Published online 28 April 2011; 10.1126/science.1199391

Fig. 1. Experimental 2D-EMD differences in LSCO between two hole doping concentrations: (**A**) Non-doped (x=0.0) - UD (x=0.08); (**B**) non-doped (x=0.0) - optimal-doped (x=0.15); (**C**) optimal-doped (x=0.15) - heavily OD (x=0.30); and (**D**) non-doped (x=0.0) - heavily OD (x=0.30). (**E**) Error map of the difference 2D-EMDs (the errors are typically 10 times smaller than the amplitudes in the 2D-EMD differences except very close to the origin).

Fig. 2. Directional symmetry of Cu-O octahedral molecular orbitals. 2D-EMD projected onto the xy plane of the molecular orbitals: (**A**) Diagram of the $P_{ZR}=P_{1x}-P_{2y}-P_{3x}+P_{4y}$ state; (**B**) P_{ZR} state (only O $2p_{x/y}$ orbitals); (**C**) P_{ZR} state hybridized with Cu $3d_{x^2-y^2}$; (**D**) diagram of the $P_0=P_{1x}+P_{2y}+P_{3x}+P_{4y}$ state; (**E**) P_0 state (only O $2p_{x/y}$ orbitals); (**F**) P_0 state hybridized with Cu $3d_{z^2}$.

Fig. 3. Theoretical electronic structure: (**A**) Band structure; (**B**) anisotropy of Compton profiles; (**C**) 2D-EMD contribution between -0.4 eV and +0.1 eV; (**D**) 2D-EMD contribution between -0.8 eV and -0.4 eV, and (**E**) 2D-EMD contribution between -0.8 eV and +1.3 eV.

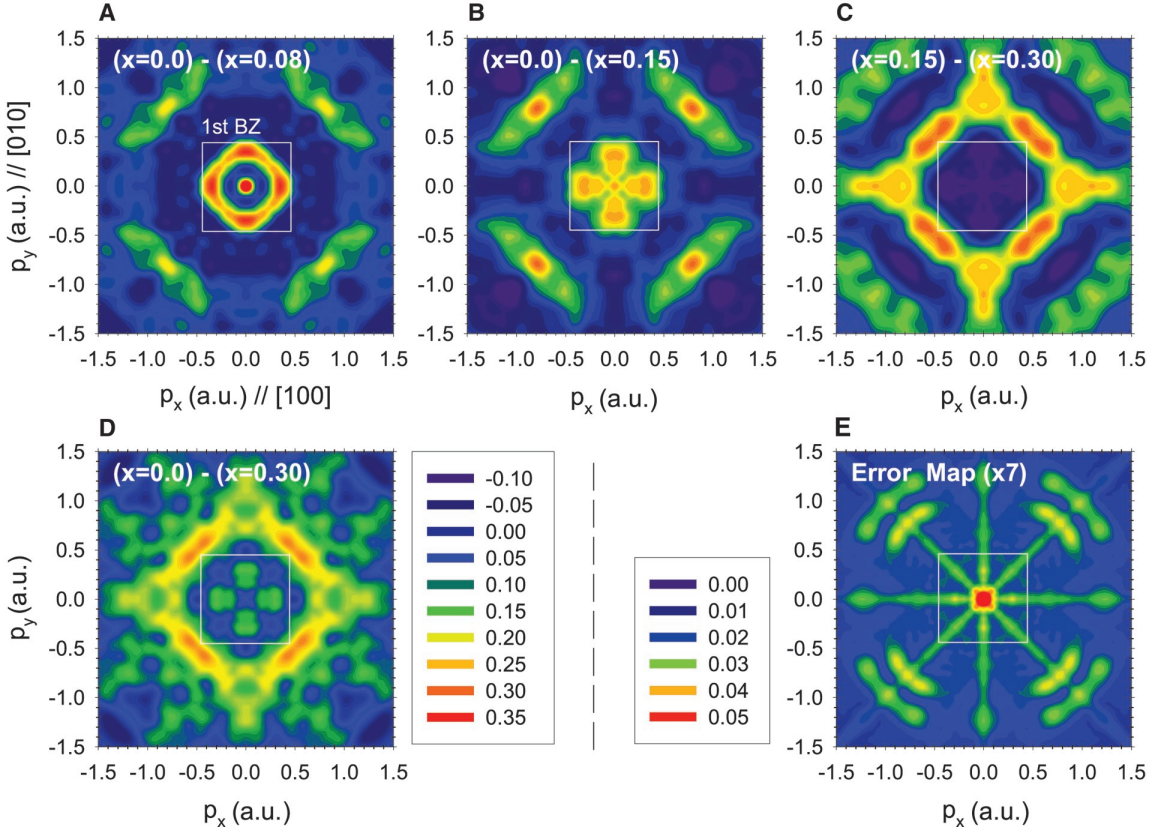
A
(x=0.0) - (x=0.08)
1st BZ
B
(x=0.0) - (x=0.15)
C
(x=0.15) - (x=0.30)
D
(x=0.0) - (x=0.30)
E
Error Map (x7)
p_y (a.u.) // [010]
p_x (a.u.) // [100]
p_x (a.u.)
p_y (a.u.)
-0.10
-0.05
0.00
0.05
0.10
0.15
0.20
0.25
0.30
0.35
0.00
0.01
0.02
0.03
0.04
0.05

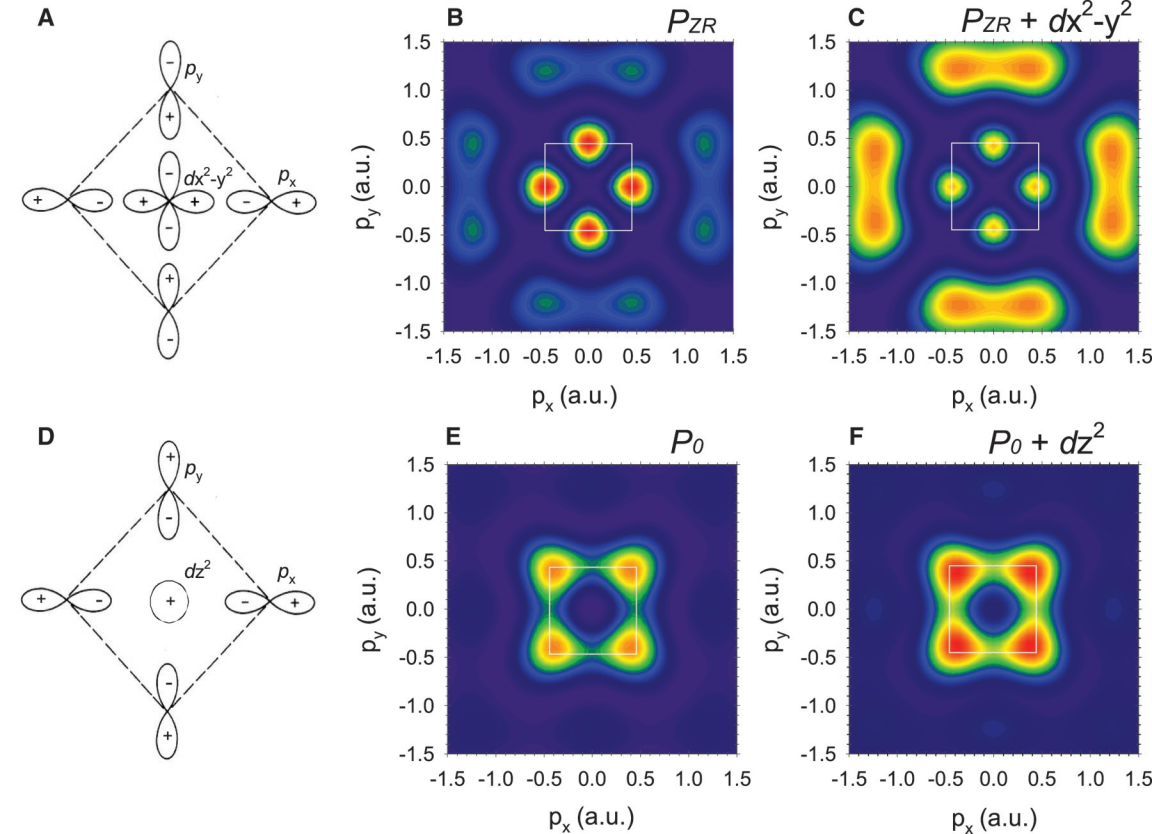
A
p_y
dx^2-y^2
p_x
B
P_{ZR}
C
P_{ZR} + dx^2-y^2
D
p_y
dz^2
p_x
E
P_0
F
P_0 + dz^2
p_y (a.u.)
p_x (a.u.)
1.5
1.0
0.5
0.0
-0.5
-1.0
-1.5

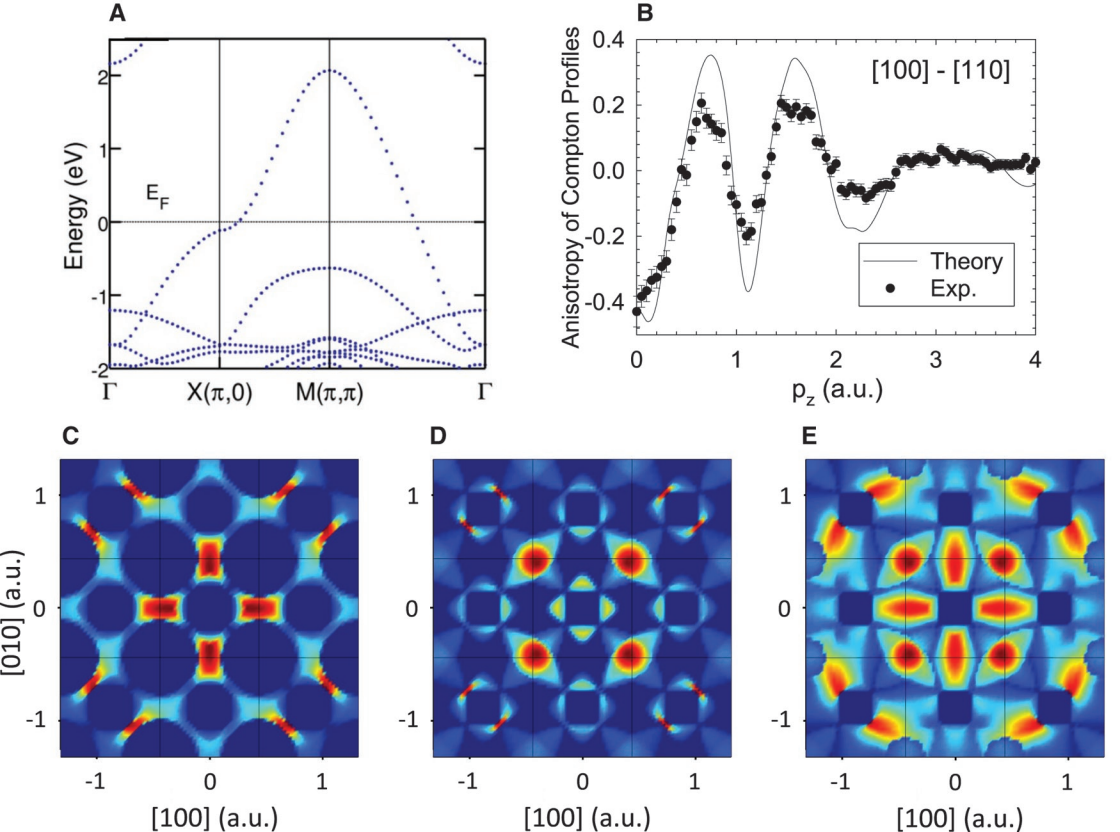
A
Energy (eV)
E_F
Γ
X(π,0)
M(π,π)
Γ
B
Anisotropy of Compton Profiles
[100] - [110]
Theory
Exp.
p_z (a.u.)
C
D
E
[010] (a.u.)
[100] (a.u.)
[100] (a.u.)
[100] (a.u.)

Imaging Doped Holes in a Cuprate Superconductor with High-Resolution Compton Scattering

Y. Sakurai, M. Itou, B. Barbiellini, P. E. Mijnarends, R. S. Markiewicz, S. Kaprzyk, J.-M. Gillet, S. Wakimoto, M. Fujita, S. Basak, Yung Jui Wang, W. Al-Sawai, H. Lin, A. Bansil and K. Yamada (April 28, 2011)
published online April 28, 2011

Editor's Summary

Science (print ISSN 0036-8075; online ISSN 1095-9203) is published weekly, except the last week in December, by the American Association for the Advancement of Science, 1200 New York Avenue NW, Washington, DC 20005.